EEET ECOLOGICAL ENGINEERING & ENVIRONMENTAL TECHNOLOGY

Ecological Engineering & Environmental Technology, 2026, 27(2), 156–169
https://doi.org/10.12912/27197050/217186
ISSN 2719–7050, License CC-BY 4.0

Received: 2025.01.07
Accepted: 2025.01.30
Published: 2026.02.07

Landslide hazard modeling using the artificial neural network approach in the Biang Loe River watershed

Andang Suryana Soma[1*], Nilam Cahyani Putri Saharudin[1], Muhammad Dandy Rachmat Ramadhan[1]

[1] Faculty of Forestry, Hasanuddin University, Jalan Perintis Kemerdekaan Km. 10, Makassar, Indonesia
* Corresponding author's e-mail: s_andangs@unhas.ac.id

ABSTRACT

The Bantaeng Regency has an extreme topography and is located in a district prone to landslides. In addition, many watersheds have been damaged in the Bantaeng Regency area, one of which is the Biang Loe watershed. This study maps landslide vulnerability using an artificial neural network (ANN) model to provide a robust predictive framework for disaster mitigation. This study was conducted to identify the distribution of landslides in the Biang Loe watershed, analyze the factors that affect the occurrence of landslides and map the level of landslide vulnerability. Analysis of 103 landslide events (2018–2022) revealed that slope direction, lithology, slope steepness, curvature, and proximity to rivers are the primary drivers of instability. The model demonstrated high predictive performance with an area under the curve (AUC) of 0.811, categorizing it as "good" for regional hazard assessment. Results show that while 25.84% of the area falls into the very low vulnerability class, critical high-risk zones were identified in areas with slopes >45% and concave curvature. These findings provide a data-driven basis for regional risk management, enabling planners to prioritize slope stabilization and restrict infrastructure development in identified high-vulnerability corridors to minimize future economic and human losses.

Keywords: artificial neural network, landslide, mapping, Biang Loe watershed.

INTRODUCTION

Human intervention has an impact on disrupting the balance of global natural ecosystems, including climate change (World Economic Forum, 2023). The greenhouse effect of increasing emissions and deforestation for various purposes is one of the causes of climate change resulting from human activities (Ali et al., 2014; Chancel et al., 2023; Gulev et al., 2021). IPCC (2023) reported that the greenhouse effect and deforestation contributed to a 1.1 °C increase in temperature from 2011–2020. The significant changes experienced are extreme climates with varied and more intense rainfall patterns in most parts of the world as well as increased extreme heat (Easterling et al., 2000; Karl et al., 1995; Seneviratne et al., 2023). Climate is a key factor that affects the environment, socioeconomic conditions, and availability of water resources (Fentaw et al., 2017; Panditharathne et al., 2023).

Climate change, as an influence on current environmental conditions, has an impact on increasing hydro-meteorological disasters. ASEAN Coordinating Centre for Humanitarian Assistance (AHA Centre) year 2023 (ASEAN Coordinating Centre for Humanitarian Assistance (AHA Centre), 2023) In his report, a total of 88 natural disasters occurred in Southeast Asia from January to August 2023, with Indonesia being prone to natural disasters. In 2022, the National Disaster Management Agency released the Indonesian Disaster Risk Index, which states that all provinces in Indonesia are at moderate to high risk of natural disasters (Adi et al., 2023). Compared with geological and biological disasters, hydro-meteorological disasters account for approximately 75% of the damage, including casualties and economic and infrastructure damage (Jayawardena, 2015).

This situation returns to human intervention, which has been active in changing the natural landscape to meet needs, resulting in the acceleration of environmental degradation, namely, deforestation, which is not balanced by the government's ability to rehabilitate forests (Murdiyarso et al., 2015; Oumer, 2009; Putra et al., 2021). Hydro-meteorological disasters include cyclones, droughts, floods, heat waves, heavy snowfall, storms, floods and forest fires, where landslides become frequent disasters.

Indonesia's mountainous conditions with extreme topography are characteristic of the natural landscape with frequent landslide phenomena. In general, landslides are defined as the movement of soil, rock and other organic matter on slopes that are affected by gravity (Highland and Bobrowsky, 2008). The triggers are the occurrence of heavy rain resulting from climate change, earthquakes, erosion and slope cutting at angles ranging from approximately 5 to 20 degrees (Bandara et al., 2013). This phenomenon is certainly also influenced by human activities related to land use (Highland and Bobrowsky, 2008; Mohammadi et al., 2018). This phenomenon is interesting for researchers studying landslides as objects and mapping their vulnerability to minimize the impact caused.

While hydro-meteorological events—including cyclones, floods, and forest fires—account for 75% of total disaster damage in terms of casualties and infrastructure, landslides remain one of the most frequent and destructive phenomena in mountainous landscapes. Currently, geographic information systems (GIS) integrated with probabilistic models like logistic regression, analytical hierarchy process (AHP), and artificial neural networks (ANN) are established tools for mapping landslide vulnerability. Methods and analysis techniques for modeling landslide vulnerability have developed continuously from time to time. GIS, which maps landslide vulnerability with remote sensing data, is able to map landslide events and their causal parameters (Mersha and Meten, 2020; Shahabi and Hashim, 2015). Many studies have combined GIS with probabilistic models, such as frequency ratios, fuzzy logic, logistic regression, certainty factors, AHPs and ANNs (Anbalagan et al., 2015; Caniani et al., 2008; Deng et al., 2017; Khaddari et al., 2023; Lee and Pradhan, 2006; Mirdda et al., 2019; Pradhan et al., 2009; Pradhan and Lee, 2010; Rasyid et al., 2016; Sema et al., 2017; Soma and Kubota, 2017, 2018; Xiong et al., 2018; Yalcin et al., 2011).

However, a critical gap remains in localized modeling: broader regional studies often overlook the specific interplay between rapid, small-scale land-cover changes and traditional geomorphic mechanics. Furthermore, many existing models rely on lower-resolution data that fail to capture the unique regional geomorphic behavior of critical areas like the Biang Loe watershed. There is a scientific need to determine how high-resolution elevation data combined with multi-temporal imagery can improve the predictive accuracy of ANN models in specific mountainous contexts.

This study uses an ANN, which is a model for mapping landslide vulnerability in the Biang Loe watershed. The ANN model was developed with information processing techniques inspired by the way biological systems, especially the human brain, work to solve a problem (Másson and Wang, 1990). The primary objectives are to evaluate the model's effectiveness in this context and to identify which causal parameters—derived from image interpretation and field surveys—contribute most significantly to landslide occurrence. Landslide history and causal data were integrated into a GIS using a 10 × 10 m raster resolution. Ultimately, this study aims to model and describe the spatial distribution of landslide vulnerability across the watershed.

METHODS

Study area

The Biang Loe watershed is in Bantaeng Regency, South Sulawesi Province, Indonesia (Figure 1). The Bantaeng Regency has an extreme topography and is in a district prone to landslides. In addition, many watersheds have been damaged in the Bantaeng Regency area, one of which is the Biang Loe watershed. Research on the watershed is linked to hydrological processes that experience an imbalance in water use so that the Biang Loe watershed ecosystem is prone to landslides.

Landslide inventory

The collection of landslide event data is very important in the analysis of landslide vulnerability. This observation was carried out by identifying landslides from the results of remote sensing image interpretation on the basis of spectral characteristics, shape, and contrast (Soma et al.,

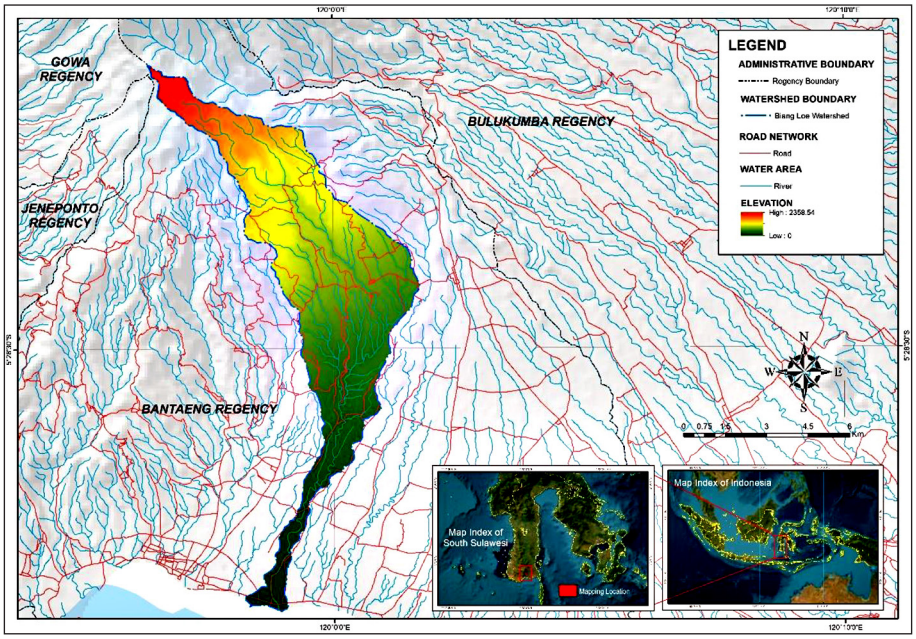

Figure 1. Research location

2019a). Landslide events from 2018–2022 were identified via the imagery time series Google Earth Pro, which has high-resolution imagery for landslide identification (Saha et al., 2021). The results of the identification are then validated to obtain high accuracy. The results of the validation as a historical database of landslide events are divided into two data camps, namely, training data and data validation. The data used for training were processed with models, whereas the data used as data testers for validation were used to assess the prediction level of the model.

Factors that cause landslides

The factors were chosen on the basis of the conditions of the features of the study area, which are closely related to the causes of landslides, from the literature and the availability of data for the study area (Caniani et al., 2008; Sdao et al., 2013; Soma et al., 2019a). The causative factors are derived from secondary and primary data processed via ArcGIS. The causative factors that are variables in this study are rainfall data, slope, distance from rivers, lithology, elevation, distance from faults, land cover, aspect (slope direction) and curvature. Rainfall is a triggering factor for landslides. Rainfall data were processed from NASA's MERRA-II climate data with a distribution of CSIRO station points. Spatial depiction of rainfall via the Isohyet method. DEM data, namely, DEMNAS data with a pixel resolution of 8 × 8 m, are used for factor data related to topographic elements, namely, slope, distance from the river, elevation, aspect and curvature. The slope is obtained through tools slope in GIS with data classifications of 0–8% (flat), 8–15% (sloping), 15–25% (slightly steep), 25–45% (steep) and >45% (very steep). The distance from the river is processed through tools to obtain the river channel and Euclidean distance to determine the distance with classifications of 0–20 m, 20–40 m, 40–60 m, 60–80 m, 80–100 m and >100 m. The elevation values at the DEM were extracted and classified with a distance interval of 250 m. The aspect was treated from the tool perspective. The curvature is treated as tool curvature with convex, flat and concave classes. Lithology data and fault lines were obtained from the geological data of the Geological Agency, Ministry of Energy and Mineral Resources of Indonesia. Advanced processing to obtain the distance from the fault is carried out with the Euclidean distance tool with an interval of 500 m. Land cover data are obtained from the results of Sentinel-2A image interpretation in 2022.

Data processing

Data management uses a qualitative method in which simple statistical techniques are used to determine the proximity between the relationships between landslide events and their causative factors. This method can be applied with a frequency ratio approach and then models an

ANN. The frequency ratio is the comparison of the area where landslides occurred in the entire study area and the comparison of the chance of landslides with those that did not experience landslides (Tazik et al., 2014). If the resulting value is greater than 1.0, then the relationship between the landslide event and the causative factor is greater, and if the ratio is less than 1.0, then the relationship between the landslide event and the causative factor is low (Lee and Lee, 2006). The ratio value in each class shows the level of relationship between the frequency value of the ratio calculated by the formula. Here, the equation used is as follows (Soma et al., 2019b):

$$Fr = \frac{PxcL\ (nm)/\sum PxcL}{Pixel\ (nm)/\sum Pnx} \quad (1)$$

where: *Fr* – Frequency ratio value, *Pxcl* – Number of pixels with landslides in class n of parameter m (nm), *Pixels* – Number of pixels in class n of parameter m (nm), *ΣPxcl* – Total pixel avalanche, *ΣPnx* – Total number of pixels in the area.

Furthermore, the results of the normalized value data from the frequency ratio were used to advance the data analysis. The value of normalization can be calculated via the following equation (Soma et al., 2019b):

$$X_i' = \left(\frac{Xi - x\ min}{x\ max - min}\right)(x'\ \max - x'\ min) + \\ + x'\ \min \quad (2)$$

where: *Xi*' – Normalized frequency ratio value, *Xi* – Frequency value ratio of each class, *Xmax* – Highest actual input data, *Xmin* – Lowest actual input data, *X'max* – Highest target value, *X'min* – Lowest target value.

Then, process that number (if it exceeds the neuron threshold, the neuron is then activated) using a nonlinear activation function to produce a result (yi), which is the output with the equation (Soma et al., 2019b):

$$yi = G + (b^2 + W^2\,(s(x^1 + W'i))) \quad (3)$$

where: yi – Results from ANN, G – Activation function, $b1$ – Bias vector 1, $W1$ – Weight matrix 1, $b2$ – Bias vector 2, $W2$ – Weight matrix 2.

The results of the analyzed data are scaled in a range from 0–1. Scaling is performed to improve the accuracy of subsequent digital information and achieve better results (Sheela and Deepa, 2013). In this study, a multilayer perceptron (MLP) was applied. For each hidden neuron and output neuron, its input is processed by multiplying each input (xi) by the appropriate weight (wi) (Soma et al., 2019b):

$$LSI\ ANN_{i=0}^{n} = \sum wixi \quad (4)$$

where: *LSI ANN* – Landslide susceptibility index/ landslide vulnerability end map calculated for all pixels, *Wi* – Input weight, *Xi* – Input.

ANN Configuration and Platform The ANN model was implemented using a multilayer perceptron (MLP) architecture within the SPSS software environment. The network configuration consisted of:

- input layer: 9 causative factors (rainfall, slope, distance from river, lithology, elevation, distance from fault, land cover, aspect, and curvature).
- hidden layer: A single hidden layer with a sigmoid activation function to process non-linearities.
- output layer: A single neuron using a linear activation function to generate the landslide susceptibility index (LSI).
- training parameters: The model utilized a backpropagation algorithm with a learning rate of 0.1 and momentum of 0.9.

The selection of iterations was determined by a stopping criterion based on the minimization of the mean square error (MSE); training ceased when the error on the validation set failed to improve for 10 consecutive iterations, preventing overfitting. The dataset was split landslide eveden from 175 pixel into 70% for training (131 pixels) and 30% for validation (44 pixels). This ratio is statistically justified as it provides a sufficient sample size for the backpropagation algorithm to converge while maintaining an independent subset large enough to ensure the reliability of the AUC/ROC validation.

Data validation

ANN modeling is used to verify the results of landslide hazard analysis via the data obtained to determine the accuracy of the map. These data determine the value of conformity by using field validation data, which provide an estimate that

field data are considered correct and most suitable for actual risk conditions. The validation results show that the prediction accuracy value is based on the area under the curve (AUC) through receiver operating characteristic (ROC) analysis via SPSS software. These data determine the validation value of the data application via estimates provided by the field. Field data are considered to be the correct and most appropriate true risk profile. In the classification, the results of landslide validation are then grouped into several value ranges, namely, 0.5 - 0.6 declared failed, 0.6–0.7 declared poor, 0.7–0.8 declared moderate/adequate, 0.8–0.9 declared good, and 0.9–1 declared very good (Rasyid et al., 2016).

Landslide vulnerability map

Furthermore, after obtaining the LSI score and going through the validation stage, a landslide susceptibility map was constructed with the level of landslide vulnerability consisting of 5 classes, namely, very low, low, medium, high, and very high. The determination of this class uses the natural breaks model.

DISCUSSION AND RESULTS

Landslide identification

There were 103 landslide incidents over 5 years (2018–2022). Identification is based on interpretation of the shape of the direction of the landslide, the slope and the hue/color of the landslide, which has a varying area (Soma et al., 2019a). The inventory was carried out from upstream, middle, and downstream areas and revealed 31 incidents with an area of 0.723 ha in 2018; 27 incidents with an area of 0.545 ha in 2019; 20 incidents with an area of 0.221 ha in 2022; and 15 incidents in 2020 with an area of 0.172 ha and 10 incidents in 2021 with an area of 0.119 ha (Figure 2).

Landslides encountered in the field are classified as traditional landslides because the rocks that move in their plane form flat or undulating slopes. The results of data processing will continue with topology test analysis to overcome errors, which are then converted into raster data, which will later be used as a database in modeling. The data division used to validate the model success rate in calculating the landslide opportunity value is 70% for model training data of 131 pixels and 30% for validation data of 44 pixels, with a total of 175 pixels out of the total pixels of the Biang Loe watershed of 4,746.05 pixels (Figures 3, 4).

Causative factors of landslides

There are 9 (nine) maps of landslide occurrence factors. The factors used in this study were the causes of landslide vulnerability selected from the literature, data availability, and conditions of the research site (Figure 5).

Frequency ratio (FR)

When the frequency values of the ratio and normalization values with the factors causing landslides are shown in Table 1, the highest FR value is found for the curvature factor of the earth in the concave class, with an FR value of 3.51, which indicates that this class has a very high chance of landslide events. This finding is in line with the findings of Rasyid et al., (2016), who reported that the FR ratio value is correlated with landslides and each class of landslide-causing factors in a numerical format.

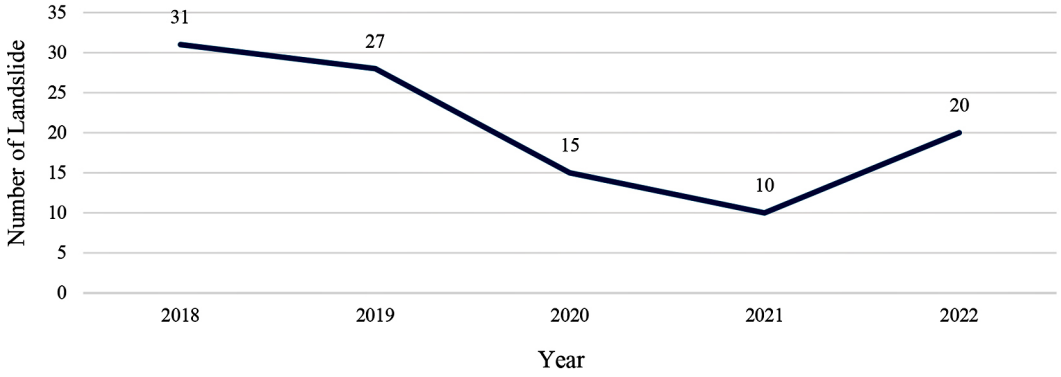

Figure 2. Graph of the number of landslide events in the Biang Loe watershed

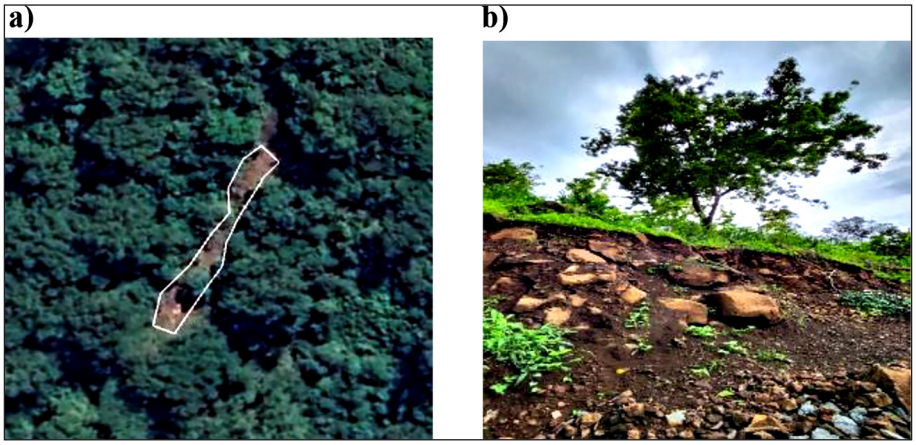

Figure 3. Form of interpretation of landslide events: (a) prediction via Google Earth Pro, (b) actual validation in the field

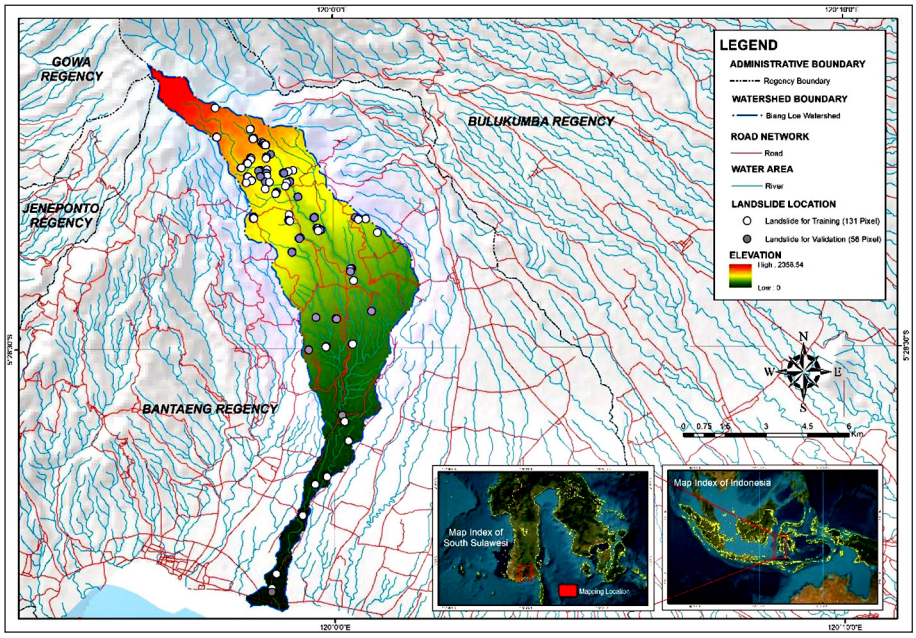

Figure 4. Map of the distribution of landslide events

Artificial neural network (ANN)

The final landslide vulnerability map is multiplied by each causative factor calculated through ANN analysis and then overlayed from these layers via the multilayer perceptron (MLP) formula with ten repetitions. From these data, the best repetition results to be taken are in the 7th (seventh) trial. The final result is determined by the LSI and tested for its validation level.

Table 2 shows that the repetition values of all the factors can affect the occurrence of landslides in this region. However, several factors strongly influence this incident. If you look at the factors that are very influential, namely, the curvature of the earth, the slope, the direction of the slope, the distance from the river and lithology. This can be attributed to the value of these factors becoming more dominant and being able to adjust to the ANN model. The ANN equation obtained in the 7th test is as follows.

$$LSI\ ANN_{iterasi} = (0.082)\ (ANN_{Tutupan\ Lahan}) + \\ + (0.096)\ (ANN_{Ketinggian}) + (0.076)\ (ANN_{Curah\ Hujan}) + \\ + (0.126)\ (ANN_{Arah\ Lereng}) + (0.106)\ (ANN_{Litologi}) + \\ + (0.145)\ (ANN_{Lereng}) + (0.149)\ (ANN_{Kelengkungan\ Bumi}) + \\ + (0.126)\ (ANN_{Jarak\ Dari\ Sungai}) + \\ + (0.093)\ (ANN_{Jarak\ Dari\ Patahan}) \quad (5)$$

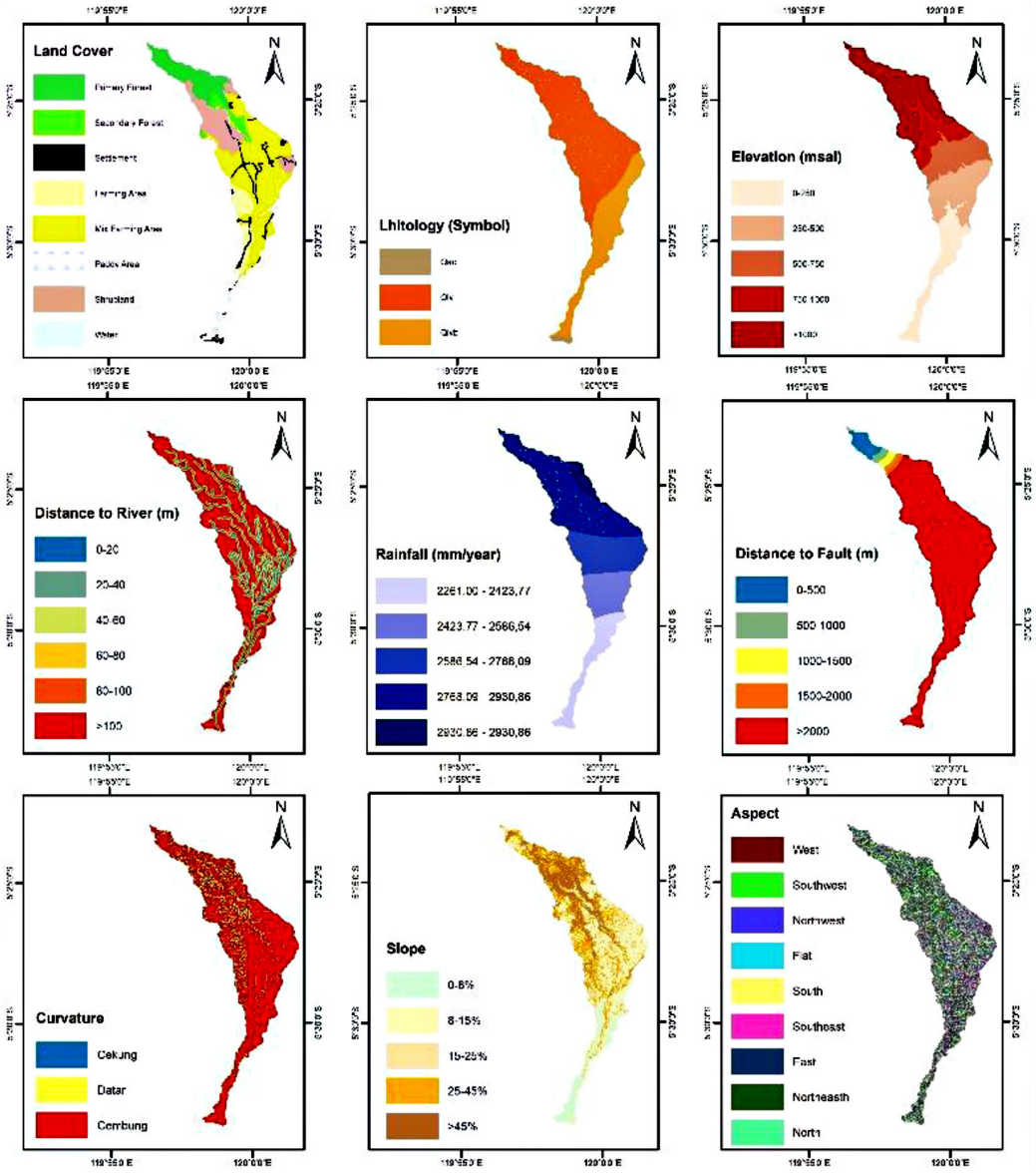

Figure 5. Map 9 landslide factors: (a) land cover, (b) lithology, (c) elevation, (d) distance from river, (e) rainfall, (f) distance from fault, (g) curvature, (h) slope and (i) aspect

The landslide vulnerability index value from the LSI ANN in Figure 8 is the best range from 0.437–1.970, and the landslide vulnerability index map is input and classified into 5 (five) classes via tools (natural breaks). The results of the data processing produce classes ranging from very low, low, medium, high and very high to landslide vulnerability (Figure 6).

Validation

Validation is carried out via the receiver operating characteristic (ROC) curve for multiclass classification. The result of this validation is the accuracy of the prediction evaluated on the basis of the area under the curve (AUC). In the research of Samanta et al., (2018), the AUC is considered a pe indicator in support of model prediction. The next stage involves the results of the ROC analysis, which is validated. Validation 1 is used to determine the success rate of the model from the ANN value, and validation 2 is used to determine the prediction level of the model against landslide events. The curve of the validation results obtained from SPSS software with ROC analysis of the Biang Loe watershed is shown in Figure 7 and Table 3.

Table 3 shows the results of ANN modeling on landslide events, with values of 0.809 for the model success rate and 0.745 for the model prediction rate. The predictive performance of the

Table 1. FR values and normalization values with landslide-causing factors

No	Parameter	Class	Pixel (nm)	%Pixel (nm)	PxcL (nm)	%PxcL (nm)	FRI	N FR
1	Land cover	Primary forest	70.836	14.93	42	32.06	2.15	0.66
		Secondary forest	19.041	4.01	17	12.98	3.23	1.00
		Settlement	28.064	5.91	0	0.00	0.00	0.00
		Dryland agriculture	38.414	8.09	6	4.58	0.57	0.17
		Mixed dryland agriculture	204.132	43.01	17	12.98	0.30	0.09
		Paddy	29.717	6.26	4	3.05	0.49	0.15
		Bushes	76.109	16.04	45	34.35	2.14	0.66
		Water body	8.266	1.74	0	0.00	0.00	0.00
2	Lithology	Qac	4.664	0.98	0	0.00	0.00	0.00
		Qlv	337.180	71.05	121	92.37	1.30	1.00
		Qlvb	132.735	27.97	10	7.63	0.27	0.21
3	Slope (%)	0–8	74.712	15.74	8	6.11	0.39	0.13
		8–15	93.102	19.62	6	4.58	0.23	0.08
		15–25	115.489	24.34	22	16.79	0.69	0.23
		25–45	103.705	21.85	23	17.56	0.80	0.27
		>45	87.571	18.45	72	54.96	2.98	1.00
4	Curvature	Concave	24.803	5.23	24	18.32	3.51	1.00
		Fl;at	72.408	15.26	16	12.21	0.80	0.23
		Convex	377.368	79.52	91	69.47	0.87	0.25
5	Elevation (msal)	0–250	85.947	18.11	9	6.87	0.38	0.21
		250–500	101.231	21.33	8	6.11	0.29	0.16
		500–750	79.651	16.78	10	7.63	0.45	0.25
		750–1000	62.191	13.10	30	22.90	1.75	0.95
		>1000	145.559	30.67	74	56.49	1.84	1.00
6	Distance from river (m)	0–20	50.658	10.67	16	12.21	1.14	0.70
		20–40	40.083	8.45	16	12.21	1.45	0.88
		40–60	41.919	8.83	19	14.50	1.64	1.00
		60–80	37.659	7.94	13	9.92	1.25	0.76
		80–100	37.788	7.96	5	3.82	0.48	0.29
		>100	266.472	56.15	62	47.33	0.84	0.51
7	Distance from fault (m)	0–500	19.828	4.18	0	0.00	0.00	0.00
		500–1000	6.835	1.44	2	1.53	1.06	0.61
		1000–1500	6.261	1.32	3	2.29	1.74	1.00
		1500–2000	7.779	1.64	0	0.00	0.00	0.00
		>2000	433.876	91.42	126	96.18	1.05	0.61
8	Aspect	North	28.485	6.00	18	13.74	2.29	1.00
		Northeast	58.995	12.43	24	18.32	1.47	0.64
		Timur	63.366	13.35	19	14.50	1.09	0.47
		Southeast	60.044	12.65	6	4.58	0.36	0.16
		South	58.199	12.26	9	6.87	0.56	0.24
		Southwest	57.698	12.16	12	9.16	0.75	0.33
		West	62.249	13.12	21	16.03	1.22	0.53
		Northwest	57.521	12.12	12	9.16	0.76	0.33
		Datar	28.022	5.90	10	7.63	1.29	0.56
9	Rainfall (mm/yr)	2261,00–2423,77	69.571	14.66	9	6.87	0.47	0.24
		2423,77–2586,54	75.169	15.84	5	3.82	0.24	0.12
		2586,54–2768,09	110.600	23.30	10	7.63	0.33	0.17
		2768,09–2930,86	196.643	41.44	107	81.68	1.97	1.00
		2930,86–3059,19	22.596	4.76	0	0.00	0.00	0.00

Note: Pxcl (nm) is the number of pixels of the landslide, the number of pixels of pixel class n on the parameter and N FR is the normalization of the FR value.

Table 2. ROC repetition values for ANN modeling

Landslide factors	Iteration									
	1	2	3	4	5	6	7	8	9	10
Land cover	0.182	0.127	0.149	0.094	0.133	0.135	0.082	0.086	0.139	0.115
Elevation	0.130	0.171	0.123	0.072	0.111	0.094	0.096	0.072	0.084	0.094
Rainfall	0.124	0.136	0.097	0.145	0.137	0.102	0.076	0.121	0.090	0.135
Aspect	0.086	0.101	0.085	0.115	0.158	0.114	0.126	0.132	0.194	0.178
Lithology	0.032	0.058	0.027	0.045	0.059	0.043	0.106	0.148	0.060	0.026
Slope	0.192	0.139	0.102	0.106	0.107	0.087	0.145	0.099	0.205	0.183
Curvature	0.087	0.042	0.126	0.080	0.084	0.147	0.149	0.189	0.021	0.042
Distance from river	0.117	0.125	0.186	0.154	0.141	0.164	0.126	0.036	0.148	0.117
Distance from fault	0.050	0.101	0.105	0.187	0.069	0.113	0.093	0.117	0.059	0.110

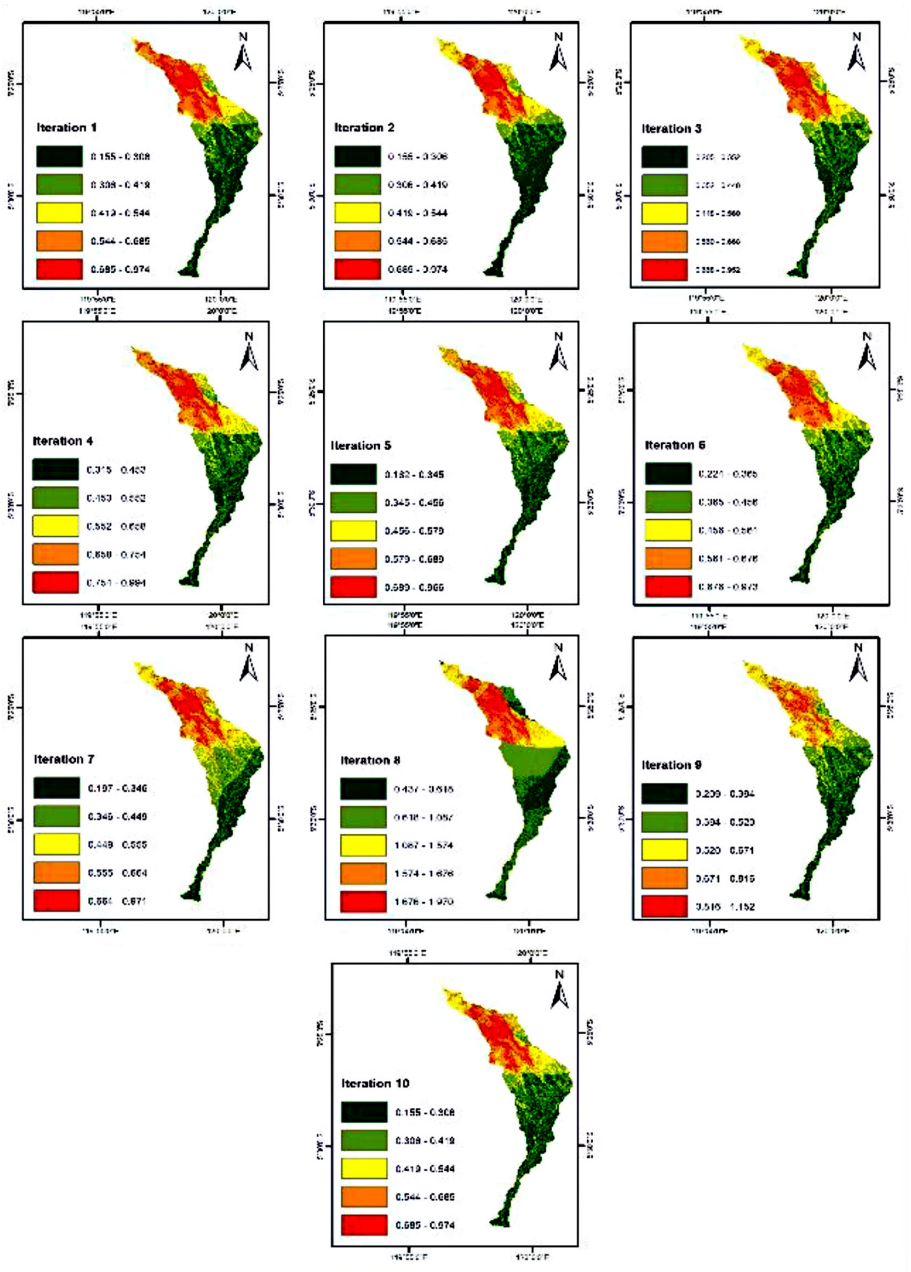

Figure 6. Landslide vulnerability index map for the ANN method

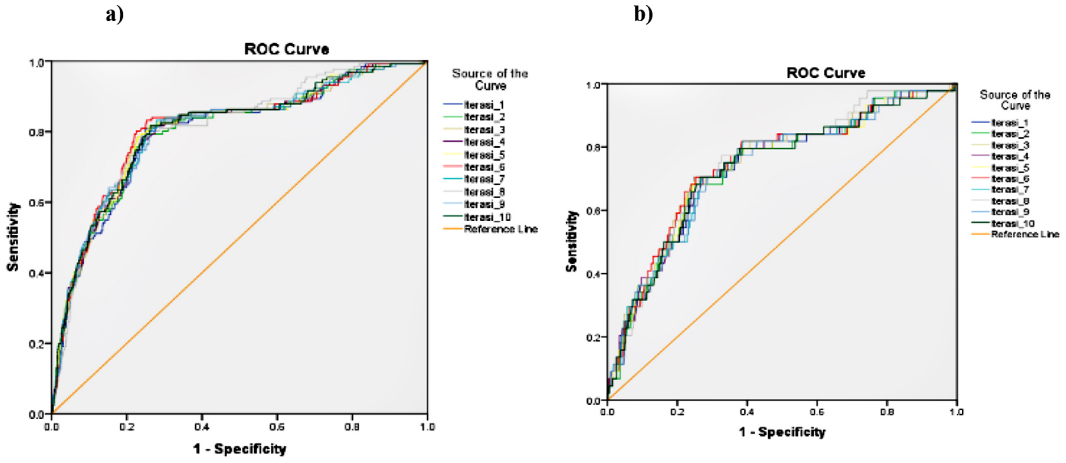

Figure 7. (a) ANN success rate and (b) prediction rate accuracy test curves

ANN model in this study (AUC: 0.809) aligns with the findings of Saha et. all (2022), who observed that neural networks provide a higher degree of accuracy in complex mountainous watersheds due to their ability to model non-linear interactions between slope and hydrology.

Landslide vulnerability map

This landslide vulnerability map is calculated on the basis of the analysis of the LSI value, which is then validated through the iteration step and then continues with the step of finding the NGO value via the class division method through the classification of natural break tools. Natural breaks are a grouping of similar values in maximizing the difference between classes (Moreira et al., 2021), which has high accuracy in the division of geographical environmental units (Basofi et al., 2015).

Table 4 shows that the landslide vulnerability index in the Biang Loe watershed can be divided into 5 (five) vulnerability classes. The most dominant landslide vulnerability is in the very low class, with areas of 1,226.30 Ha or 25.84% of the watershed area. The second is in the low class, which has an area of 1,165.04 Ha or 24.55% of the watershed area. Third, the high class has an area of 865.36 ha or 18.23% of the watershed area. Fourth, the medium class has an area of 816.21 ha or 17.20% of the watershed area. Fifth, the very high class has an area of 673.12 or 14.18% of the watershed area. On the basis of the level of vulnerability, the predominant parameters for each parameter are presented in Table 5.

Table 5 shows that in the first class, the landslide vulnerability is very low, dominated by an elevation of 0–250 m asl, the land cover of the mixed farming area, with a rainfall of

Table 3. ANN modeling AUC values from the ROC analysis results for the success rate and prediction

No	Validation	AUC value									
		1	2	3	4	5	6	7	8	9	10
1	Success	0.796	0.799	0.803	0.803	0.807	0.809	0.805	0.808	0.804	0.805
2	Predictions	0.734	0.733	0.742	0.736	0.737	0.745	0.737	0.744	0.732	0.732

Table 4. Vulnerability index values and classes

No	Vulnerability index value	Landslide vulnerability classes	Number of pixels	Area (Ha)	(%)
1	1.82–3.14	Very low	121.610	1.226,30	25.84
2	3.14–4.12	Low	116.908	1.165,04	24.55
3	4.12–5.17	Keep	81.580	816.21	17.20
4	5.17–6.19	High	86.930	865.36	18.23
5	6.19–8.66	Very high	67.551	673.12	14.18
Sum			474.579	4.746,05	100

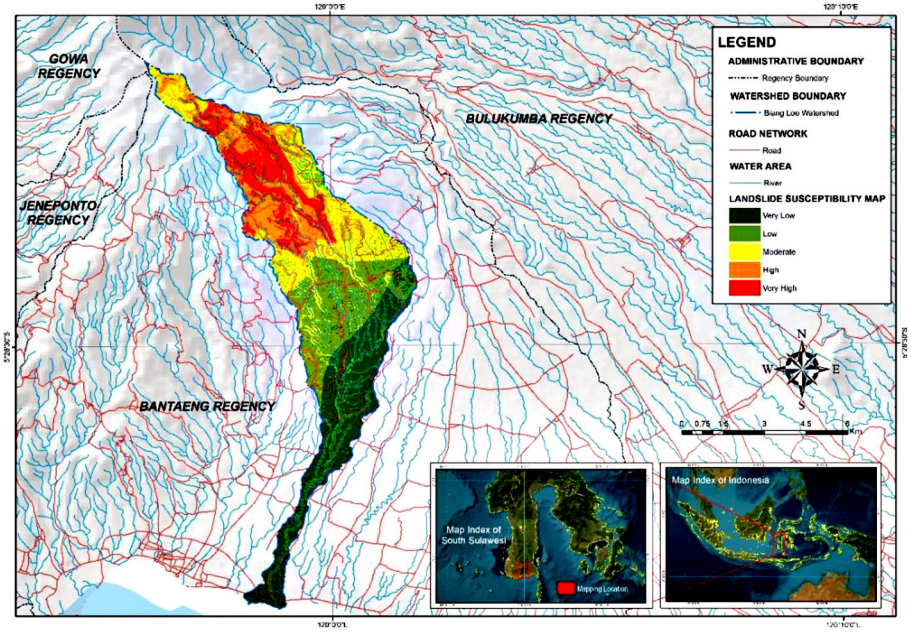

Figure 8. Map of the vulnerability level of landslides in the Biang Loe watershed

Table 5. Parameters that influence landslide vulnerability

Parameter	Vulnerability classes				
	Very low	Low	Keep	Tall	Very high
Elevation	0–250 m asl	500–750 m asl	>1000 m asl		
Land cover	Mix farming area		Scrubland		Primary and secondary forest
Rainfall	2,261.00-2,423.77 mm/yr	2,586.54-2,768.09 mm/yr	2,768.09-2,930.86 mm/yr		
Aspect	Southeast	East	North and Northeast		
Lithology	Qac dan Qlvb	Qlv			
Slope	0–8%	15–25%	25–45%		>45%
Curvature	Concave				
Distance from river	40–60 m				
Distance from fault	1500–2000 m				

2,261.00–2,423.77 mm/year, the direction of the southeast slope, the lithology of the Qac and Qlvb, the slope of 0–8%, concave curvature, the distance from the river 40–60 m and the distance from the fault of 1500–2000 m. In the second class, low landslide vulnerability is dominated by an elevation of 500– 750 m asl, mixed farming area land cover, rainfall of 2,585.54–2,768.09 mm/yr, east slope direction, Qlv lithology, slope 15–25%, concave curvature, distance from the river 40–60 m and distance from faults 1500–2000 m. In the third class, landslide vulnerability is dominated by an elevation of >1000 m asl, shrubland cover, rainfall of 2,768.09–2,930.86 mm/yr, direction of the northern and northeastern slopes, lithology of the Qlv, slope of 25–45%, concave curvature, and distance from the river 40–60 m. Based on the Table 5 show the more affect the occurrence of landslides in the Biang Loe watershed are aspect, lithology, slope, curvature and distance from the river. Furthermore, our findings regarding factor dominance mirror regional observations in South Sulawesi; for instance, Asdar et al. (2021) identified that slope steepness and lithology were primary drivers of instability in the nearby Tangka Watershed using the Frequency Ratio method. While different statistical approaches were utilized, the convergence of results highlighting topography and geology as dominant predictors across both the Biang Loe and Tangka watersheds suggests a consistent geomorphic behavior in the region. This validates the robust generalization capabilities of the ANN approach for localized disaster management and spatial planning in Indonesia.

CONCLUSIONS

The analysis of landslide distribution in the Biang Loe watershed over the last five years revealed a total of 103 distinct incidents, peaking in 2018, with 31 events covering 0.723 hectares. Through the application of the ANN model, this study determined that the structural predisposition for soil instability in this region is driven primarily by five dominant causative factors: aspect, lithology, slope steepness, curvature, and proximity to river systems. These results align with contemporary regional geomorphic behavior, confirming that high-resolution topographic and geological factors remain the primary predictors of landslide initiation in the South Sulawesi landscape.

In terms of spatial susceptibility, the ANN model demonstrated high predictive reliability in identifying critical zones of instability. The "high" vulnerability category accounts for 18.37% of the area, whereas the "very high" category encompasses 15.48%, representing zones where steep gradients and specific lithological formations intersect. Consequently, the resulting landslide susceptibility map provides a critical data-driven framework for regional risk management, offering actionable insights for local authorities to prioritize slope stabilization and refine spatial planning policies to reduce potential human and economic losses.

Acknowledgments

Appreciation is conveyed to the Faculty of Forestry of Hasanuddin University for granting permission to conduct this research.

REFERENCES

1. Ali, A., Riaz, S., Iqbal, S. (2014). Deforestation and its impacts on climate change an overview of Pakistan. *Papers on Global Change IGBP*, *21*(1), 51–60. https://doi.org/10.1515/igbp-2015-0003
2. Anbalagan, R., Kumar, R., Lakshmanan, K., Parida, S., Neethu, S. (2015). Landslide hazard zonation mapping using frequency ratio and fuzzy logic approach, a case study of Lachung valley, Sikkim. *Geoenvironmental Disasters*, *2*(1). https://doi.org/10.1186/s40677-014-0009-y
3. Asdar, Arsyad, U., Soma, A. S., Mappangaja, B., Wahyuni. (2021). Analysis of the landslides vulnerability level using frequency ratio method in Tangka Watershed. *IOP Conference Series: Earth and Environmental Science, 870*(1), 012013. https://doi.org/10.1088/1755-1315/870/1/012013
4. ASEAN Coordinating Centre for Humanitarian Assistance (AHA Centre). (2023). *Road to Ardex-23: Final Exercise Planning Team (EPT) Meeting and Referee Training for the ASEAN Regional Disaster Emergency Response Simulation Exercise 2023 in The Column MONTHLY* 82, Issue May.
5. Bandara, R. M. S., Somarathna, M., Indrathilaka, L., Amarathunga, N., Tsukamoto, S., Fujisawa, S., Tozawa, M., Uchikura, Y. (2013). *The Manual of Landslide Monitoring, Analysis and Countermeasures*. NBRO & JICA DiMCEP. http://open_jicareport.jica.go.jp/pdf/12112116_05.pdf
6. Basofi, A., Fariza, A., Ahsan, A. S., Kamal, I. M. (2015). A Comparison Between Natural and Head/Tail Breaks in LSI (Landslide Susceptibility Index) Classification for Landslide Susceptibility Mapping: A Case Study in Ponorogo, East Java, Indonesia. *2015 International Conference on Science in Information Technology: Big Data Spectrum for Future Information Economy, ICSITech 2015*, 337–342. https://doi.org/10.1109/ICSITech.2015.7407828
7. Caniani, D., Pascale, S., Sdao, F., Sole, A. (2008). Neural networks and landslide susceptibility: a case study of the urban area of Potenza. *Natural Hazards*, *45*(1), 55–72. https://doi.org/10.1007/s11069-007-9169-3
8. Chancel, L., Bothe, P., Voituriez, T. (2023). *Climate Inequality Report 2023, World Inequality Lab Study 2023/1*. World Inequality Lab Study.
9. Deng, X., Li, L., Tan, Y. (2017). Validation of spatial prediction models for landslide susceptibility mapping by considering structural similarity. *ISPRS International Journal of: Geo-Information*, *6*(103). https://doi.org/10.3390/ijgi6040103
10. Easterling, D. R., Meehl, G. A., Parmesan, C., Changnon, S. A., Karl, T. R., Mearns, L. O. (2000). Climate extremes: observations, modeling, and impacts. *Science's Compass*, *289*, 2068–2074.
11. Fentaw, F., Hailu, D., Nigussie, A. (2017). Trend and variability analysis of rainfall stream flow series at Tekeze River Basin, Ethiopia. *International Journal of Scientific & Engineering Research*, *8*(11), 665–680. http://www.ijser.org
12. Gulev, S. K., Thorne, P. W., Ahn, J., Dentener, F. J., Domingues, M. C., Gerland, S., Gong, D., Kaufman, D. S., Nnamchi, H. C., Quaas, J., Rivera, J. A., Sathyendranath, S., Smith, S. L., Trewin, B., von Schuckmann, K., Vose, R. S. (2021). The Changing State of the Climate. In *Climate Change 2021: The Physical Science Basis, Contribution of Working Group I to the Sixth Assessment Report of the Intergovernmental Panel on Climate Change* 287–422. Cambridge University Press. https://doi.org/10.1017/9781009157896.004.288
13. Highland, L. M., Bobrowsky, P. (2008). The

Landslide Handbook - A guide to Understanding Landslides. In *US Geological Survey Circular* (Issue 1325). US Geological Survey Circular.

14. IPCC. (2023). *Climate Change 2023: Synthesis Report. Contribution of Working Groups I, II and III to the Sixth Assessment Report of the Intergovernmental Panel on Climate Change*. IPCC. https://www.unep.org/resources/report/climate-change-2023-synthesis-report
15. Jayawardena, A. W. (2015). Hydrometeorological disasters: causes, effects and mitigation measures with special reference to early warning with data driven approaches of forecasting. *Procedia IUTAM*, *17*, 3–12. https://doi.org/10.1016/j.piutam.2015.06.003
16. Karl, T. R., Knight, R. W., Easterling, D. R., Quayle, R. G. (1995). Trends in Y.S Climate During the Twentieth Century. *Conseq*, *1*, 3–12.
17. Khaddari, A., Jari, A., Chakiri, S., El Hadi, H., Labriki, A., Hajaj, S., Goumghar, L., El Harti, A., Abioui, M. (2023). A comparative analysis of analytical hierarchy process and fuzzy logic modeling in flood susceptibility mapping in the Assaka Watershed, Morocco. *Journal of Ecological Engineering*, *24*(8), 62–83. https://doi.org/10.12911/22998993/165958
18. Lee, G.-S., Lee, K.-H. (2006). Scaling effect for estimating soil Ioss in the RUSLE model using remotely sensed geospatial data in Korea. *Hydrology and Earth System Sciences Discussions*, *3*(1), 135–157. https://doi.org/https://doi.org/10.5194/hessd-3-135-2006
19. Lee, S., Pradhan, B. (2006). Landslide hazard mapping at Selangor, Malaysia using frequency ratio and logistic regression models. *Landslides*, *4*(1), 33–41. https://doi.org/10.1007/s10346-006-0047-y
20. Másson, E., Wang, Y. J. (1990). Introduction to computation and learning in artificial neural networks. *European Journal of Operational Research*, *47*(1), 1–28. https://doi.org/10.1016/0377-2217(90)90085-P
21. Mersha, T., Meten, M. (2020). GIS-based landslide susceptibility mapping and assessment using bivariate statistical methods in Simada Area, Northwestern Ethiopia. *Geoenvironmental Disasters*, *7*(1). https://doi.org/10.1186/s40677-020-00155-x
22. Mirdda, H. A.., Bera, S., Siddiqui, M. A., Singh, B. (2019). Analysis of bivariate statistical and multicriteria decision-making models in landslide susceptibility mapping in lower Mandakini Valley, India. *GeoJournal*. https://doi.org/10.1007/s10708-019-09991-3
23. Mohammadi, A., Shahabi, H., Bin Ahmad, B. (2018). Integration of INSAR technique, google earth images and extensive field survey for landslide inventory in a part of Cameron Highlands, Pahang, Malaysia. *Applied Ecology and Environmental Research*, *16*(6), 8075–8091. https://doi.org/10.15666/aeer/1606_80758091
24. Moreira, L. L., de Brito, M. M., Kobiyama, M. (2021). Effects of different normalization, aggregation, and classification methods on the construction of flood vulnerability indexes. *Water (Switzerland)*, *13*(1). https://doi.org/10.3390/w13010098
25. Murdiyarso, D., Purbopuspito, J., Kauffman, J. B., Warren, M. W., Sasmito, S. D., Donato, D. C., Manuri, S., Krisnawati, H., Taberima, S., Kurnianto, S. (2015). The potential of Indonesian mangrove forests for global climate change mitigation. *Nature Climate Change*, *5*(12), 1089–1092. https://doi.org/10.1038/nclimate2734
26. Oumer, H. A. (2009). *Land Use and Land Cover Change, Drivers and Its Impact: A Comparative Study From Kuhar Michael and Lenche Dima of Blue Nile and Awash Basins of Ethiopoa* (Issue August). Cornell University.
27. Panditharathne, R., Gunathilake, M. B., Chathuranika, I. M., Rathnayake, U., Babel, M. S., Jha, M. K. (2023). Trends and variabilities in rainfall and streamflow: A case study of the Nilwala River Basin in Sri Lanka. *Hydrology*, *10*(8), 1–17. https://doi.org/10.3390/hydrology10010008
28. Pradhan, B., Lee, S. (2010). Landslide susceptibility assessment and factor effect analysis: backpropagation artificial neural networks and their comparison with frequency ratio and bivariate logistic regression modeling. *Environmental Modeling and Software*, *25*(6), 747–759. https://doi.org/10.1016/j.envsoft.2009.10.016
29. Pradhan, B., Lee, S., Buchroithner, M. F. (2009). Use of geospatial data and fuzzy algebraic operators to landslide-hazard mapping. *Appl Geomat*, *1*, 3–15. https://doi.org/10.1007/s12518-009-0001-5
30. Putra, A., Dewata, I., Gusman, M., Author, C. (2021). Literatures reviews: Hydrometeorological disasters and climate change adaptation efforts. *Sumatra Journal of Disaster, Geography and Geography Education*, *5*(1), 7–12.
31. Rasyid, A. R., Bhandary, N. P., Yatabe, R. (2016). Performance of frequency ratio and logistic regression model in creating GIS based landslides susceptibility map at Lompobattang Mountain, Indonesia. *Geoenvironmental Disasters*, *3*(19). https://doi.org/10.1186/s40677-016-0053-x
32. Saha, S., Roy, J., Hembram, T. K., Pradhan, B., Dikshit, A., Abdul Maulud, K. N., Alamri, A. M. (2021). Comparison between deep learning and tree-based machine learning approaches for landslide susceptibility mapping. *Water (Switzerland)*, *13*(19). https://doi.org/10.3390/w13192664
33. Saha, A., Villuri, V. G. K., Bhardwaj, A. (2022). Development and assessment of GIS-based landslide susceptibility mapping models using ANN,

Fuzzy-AHP, and MCDA in Darjeeling Himalayas, West Bengal, India. *Land*, 11(10), 1711. https://doi.org/10.3390/land11101711

34. Samanta, S., Pal, D. K., Palsamanta, B. (2018). Flood susceptibility analysis through remote sensing, GIS and frequency ratio model. *Applied Water Science*, *8*(2), 1–14. https://doi.org/10.1007/s13201-018-0710-1
35. Sdao, F., Lioi, D. S., Pascale, S., Caniani, D., Mancini, I. M. (2013). Landslide susceptibility assessment by using a neuro-fuzzy model: A case study in the rupestrian heritage rich area of Matera. *Natural Hazards and Earth System Science*, *13*(2), 395–407. https://doi.org/10.5194/nhess-13-395-2013
36. Sema, H. V., Guru, B., Veerappan, R. (2017). Fuzzy gamma operator model for preparing landslide susceptibility zonation mapping in parts of Kohima Town, Nagaland, India. *Modeling Earth Systems and Environment*, *3*(2), 499–514. https://doi.org/10.1007/s40808-017-0317-9
37. Seneviratne, S. I., Zhang, X., Adnan, M., Badi, W., Dereczynski, C., Di Luca, A., Ghosh, S., Iskandar, I., Kossin, J., Lewis, S., Otto, F., Pinto, I., Satoh, M., Vicente-Serrano, S. M., Wehner, M., Zhou, B. (2023). Weather and Climate Extreme Events in a Changing Climate. In *Climate Change 2021: The Physical Science Basis, Contribution of Working Group I to the Sixth Assessment Report of the Intergovernmental Panel on Climate Change* 1513–1765. Cambridge University Press. https://doi.org/10.1017/9781009157896.013.1514
38. Shahabi, H., Hashim, M. (2015). Landslide susceptibility mapping using GIS-based statistical models and remote sensing data in tropical environment. *Scientific Reports*, *5*, 1–15. https://doi.org/10.1038/srep09899
39. Sheela, K. G., Deepa, S. N. (2013). Review on methods to fix number of hidden neurons in neural networks. *Mathematical Problems in Engineering*, *2013*. https://doi.org/10.1155/2013/425740
40. Soma, A. S., Kubota, T. (2017). The performance of land use change causative factor on landslide susceptibility map in Ujung-Loe Watersheds South Sulawesi Indonesia. *Geoplanning: Journal of Geomatics and Planning*, *4*(2).
41. Soma, A. S., Kubota, T. (2018). Landslide susceptibility map using certainty factor for hazard mitigation in mountainous areas of Ujung-Loe Watershed in South Sulawesi. *Forest and Society*, *2*(1), 79–91. https://doi.org/10.24259/fs.v2i1.3594
42. Soma, A. S., Kubota, T., Mizuno, H. (2019a). Optimization of causative factors using logistic regression and artificial neural network models for landslide susceptibility assessment in Ujung Loe Watershed, South Sulawesi Indonesia. *Journal of Mountain Science*, *16*(2). https://doi.org/10.1007/s11629-018-4884-7
43. Soma, A. S., Kubota, T., Mizuno, H. (2019b). Optimization of causative factors using logistic regression and artificial neural network models for landslide susceptibility assessment in Ujung Loe Watershed, South Sulawesi Indonesia. *Journal of Mountain Science*, *16*(2), 383–401. https://doi.org/10.1007/s11629-018-4884-7
44. Tazik, E., Jahantab, Z., Bakhtiari, M., Rezaei, A., Alavipanah, S. K. (2014). Landslide susceptibility mapping by combining the three methods Fuzzy Logic, frequency ratio and analytical hierarchy process in Dozain basin. *International Archives of the Photogrammetry, Remote Sensing and Spatial Information Sciences - ISPRS Archives, The 1st ISPRS International Conference on Geospatial Information Research, 15–17 November 2014, Tehran, Iran*, *40*(2W3), 267–272. https://doi.org/10.5194/isprsarchives-XL-2-W3-267-2014
45. W. Adi W. , A., Shalih, O., Shabrina, F. Z., Rizqi, A., Putra, A. S., Karimah, R., Eveline, F., Alfian, A., Syauqi, Septian, R. T., Widiastono, Y., Bagaskoro, Y., Dewi, A. N., Rahmawati, I., Seniarwan, Suryaningrum, H. A., Purnamasiwi, D. I., Puspasari, T. J. (2023). *IRBI (Indeks Risiko Bencana Indonesia) Tahun 2022,* 1. Badan Nasional Penanggulangan Bencana.
46. World Economic Forum. (2023). *The Global Risks Report 2023: 18th Edition* (18th Editi). World Economic Forum.
47. Xiong, T., Indrawan, I. G. B., Eka Putra, D. P. (2018). Landslide susceptibility mapping using analytical hierarchy process, statistical index, index of enthropy, and logistic regression approaches in the TinalahWatershed, Yogyakarta. *Journal of Applied Geology*, *2*(2), 67. https://doi.org/10.22146/jag.39983
48. Yalcin, A., Reis, S., Aydinoglu, A. C., Yomralioglu, T. (2011). A GIS-based comparative study of frequency ratio, analytical hierarchy process, bivariate statistics and logistics regression methods for landslide susceptibility mapping in Trabzon, NE Turkey. *Catena*, *85*(3), 274–287. https://doi.org/10.1016/j.catena.2011.01.014